Neuronal Modeling of Focality Enhancements using Steerable Subwavelength Magnetic Arrays for Transcranial Magnetic Stimulation

Matthew C. Smith
Applied Electromagnetics Research Group - Electrical Engineering
University of California San Diego
San Diego, CA 920933
mcs008@eng.ucsd.edu

Abstract

The modeling of the biophysical and bioelectromagnetic mechanisms underlying the noninvasive technique of Transcranial Magnetic Stimulation (TMS) is undertaken to better understand the excitatory and inhibitory neurodynamics within the cortical regions of the brain. After twenty years, TMS empirical results have been both encouraging and effective for both science and medical treatments, yet the foundations of the fundamental biophysical and electrophysiological models are only beginning to be understood. Several advancements are proposed which potentially offer enhanced focality by reducing the beam of magnetic field and induced electric field to a smaller target area of the cortex (<2mm^2) in lieu of the state-of-the-art at approximately 2cm^2. Also, novel techniques are formulated for reconfigurable beam steering, multiple beams and the synthesis of "custom" shape profiles in the targeted cortical region. Neuronal modeling using the active nonuniform cable equation validates the nonuniform nature of spatial excitability along nerve fibers. Thus, greater control of focality and patterning will lead to great efficacy of TMS.

1 Introduction

TMS was introduced by Anthony Barker (University of Sheffield, UK) in 1985 [1]. Over the last twenty years TMS has entered the main stream of neuro science research as a standard stimulation technique for noninvasive exploration of the interaction between excitatory and inhibitory neural activity within and between specific cortical areas of the brain. It is also being employed as a therapeutic treatment of such pathological conditions as depression, stroke, Parkinson's disease, bipolar disorder, tinnitus and pain management [2]-[4]. Despite the wide use of TMS in research the mechanism of neuronal excitation by TMS is largely unknown.

When a time-varying magnetic field ($\vec{\boldsymbol{B}}$) is propagated near a subject's head, as shown in Figure 1(a), an induced E-field intensity ($\vec{\boldsymbol{E}}$) creates eddy currents that flow through the target nerve tissue. These currents flow through the neuronal membrane creating a hyperpolarized and/or depolarized level to the resting membrane potential (V_m= -70 mV) [5]. Depolarization can reach a level where an action potential is triggered. Polarization is a function of coil design and positioning of the coil. However, it is hypothesized that many other factors are involved in determining the depolarization such as tissue non-homogeneous anisotropic components, various

conductivities of different tissues and geometric discontinuities such as points where fibers bend or change diameter, axonal boundaries, or terminal boutons.

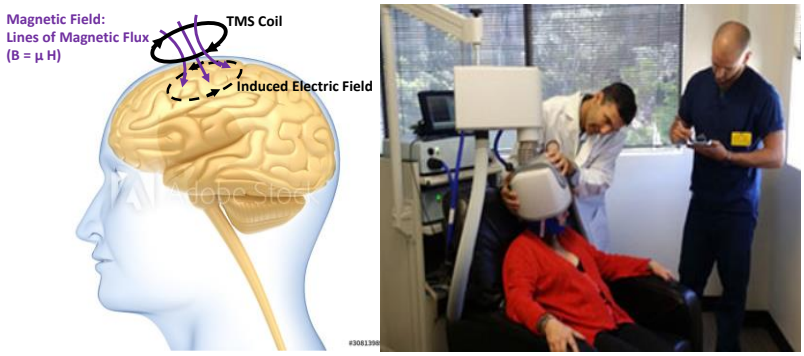

(a) **(b)**

Figure 1: (a) time-varying magnetic flux density $(\vec{B})$ induces E-field $(\vec{E})$ creates eddy currents that flow through the target nerve tissue, and (b) UCSD Dr. Feifel adjusts a FDA approved TMS device in preparation for a patient to receive TMS therapy [3]

This study starts by formulating the mechanisms of the time–varying magnetic stimulation, the induced electric field in the tissue and the response by the nerve cell. The objective is to provide a hypothesis and a clear path towards future research of biophysical modeling using an integrated Hodgkin-Huxley and active cable models using MATLAB [6] to analyze neuronal activity coupled with COMSOL [7] and HFSS [8] multiphysics models to provide an increased understanding of the problem. Also, a rudimentary lab demo was undertaken to demonstrate illustrate how 'unfocused" the magnetic field propagates through cortical tissue.

2 $(\vec{B})$ Pulses - Induced $(\vec{E})$ Fields to Cortical Neurons

A modified Hodgkin-Huxley/cable equation neuron model is used to evaluate firing patterns (ISI, AMP) of the action potential coupled with an electromagnetic solver (HFSS & COMSOL) to model the power and eddy currents delivered to the target area. Biological tissue is composed of many non-homogeneous anisotropic components, such as the cellular/axonal membrane, internal organelles and the extracellular medium. Electrical properties such as conductivity vary with location in the tissue especially at microscopic levels. These models will investigate the dynamics and that biological tissue complexities need to be integrated in to the modeling and ways to improve predictability and accuracy.

A Hodgkin-Huxley neuron model combined with the active cable model is used to evaluate eh spatial influences on the excitability of the action potential coupled with electromagnetic solvers (COMSOL and HFSS Multiphysics modules) to model the charge density and eddy currents delivered to the target area. Biological tissue is composed of many non-homogeneous anisotropic components, such as the cellular/axonal membrane, internal organelles and the extracellular medium. Electrical properties such as conductivity vary with location in the tissue especially at microscopic levels. These models will investigate the dynamics and that biological tissue complexities need to be integrated in to the modeling and ways to improve predictability and accuracy.

2.1 Magnetic Field Generation

The magnetic stimulation $(\vec{B})$ or flux density in TMS is based on Faraday's Law, equation (1), as it induces an E-field $(\vec{E})$ in neurons by an alternating current flowing through a coil. The coil or inductor used in TMS stores energy from a magnetic field when the current (I) runs through it per the Biot-Savart law in eqn. (2) [9]-[11].

$$\nabla \times \vec{E} = -\frac{\partial \vec{B}}{\partial x} \qquad (1)$$

$$d\vec{B} = \frac{\mu_o I\, d\vec{L} \times \hat{r}}{4\pi R^2} = \frac{\mu_o I\, d\vec{L} \sin(\theta)}{4\pi R^2} \qquad (2)$$

Equation (2) is simplified at an angle of 90^0 for all points along a loop with the distance being held constant to the field point from the center of the loop for magnetic flux density $\vec{B}$ in eqn. (3).

$$\vec{B} = \frac{\mu_o I}{4\pi R^2} \oint d\vec{L} = \frac{\mu_o I}{4\pi R^2}\, 2\pi R = \frac{\mu_o I}{2R} \qquad (3)$$

Using the relations in the Figure 2 a simplification of equation 2 can produce a viable approximation for the magnetic flux density $\vec{B}$ at a distance z from the center of the coil in equations (3) and (4) [9]-[11].

.

$$d\vec{B} = \frac{\mu_o I\, d\vec{L} \times \hat{r}}{4\pi R^2} = \frac{\mu_o I\, d\vec{L} \sin(\theta)}{4\pi R^2} \qquad (4)$$

$$\vec{B}_z = \frac{\mu_o 2\pi N I R^2}{4\pi (z^2 + R^2)^{3/2}}\, \hat{z} \qquad (5)$$

Figure 2(a) illustrates that for symmetry around the loop and simplification of the equation at some distance z from the center of the TMS loop to the cortical region of interest. Figure 2(b) shows calculated values, using equation (4), for two types of coils as compared to standard medical industry coils [5] with good agreement with the magnetic flux density ($\vec{B}_z$) [9]-[11].

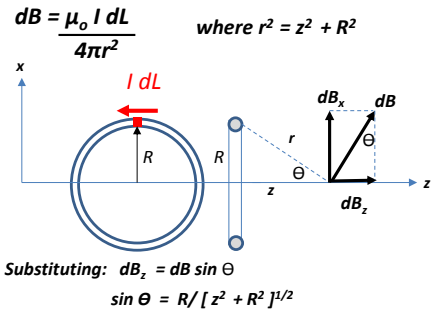

(a)

Parameter $B_z = \frac{\mu_o}{4\pi} \frac{2\pi I R^2}{(z^2 + R^2)^{\frac{3}{2}}}$	Butterfly* 	Circular* 
I(kA)/turn	3.8	3.8
# turns	18	15
Radius (R), ID (m)	.028	.020
B_z (T)	1.5	1.79
Peak B_z (T)	2.1	2.52
Peak B_z(T)[1]	2.2	2.6
B_{axial} (T) or z Cortex	0.637	0.436

* Magstim 200 (used in > 70% of neurological research and clinical therapy) @ Typ. 2.5cm Cortical Target Depth

(b)

Figure 2: (a) ($\vec{B}$) B-Field (flux density) on axis of a current loop at distance z and (b) Comparison of Standard Medical Coils* to author's calculation (blue font)

The magnetic flux density ($\vec{B}_z$) is plotted versus distance (see separate folder Appendix A for my Matlab code) in Figure 3(b) for the ideal case line showing rapid decay in strength as it moves away from the coil in the z direction axially in to an ideal medium.

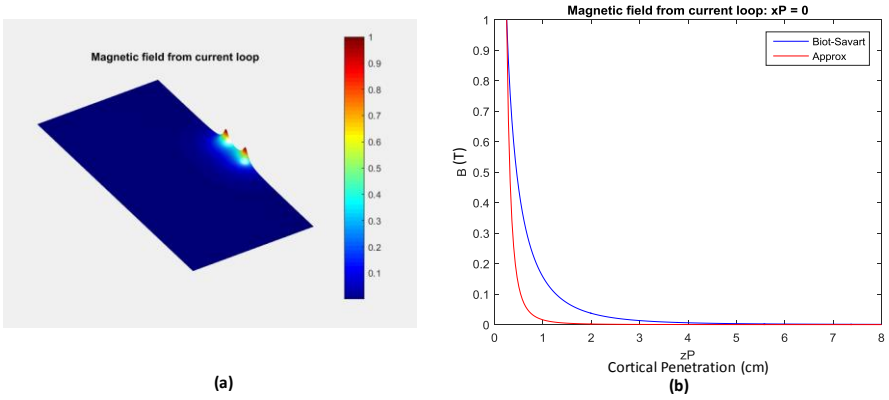

Figure 3: (a) ($\vec{B}$) B-Field (flux density) on axis of a current loop at distance z and (b) Rapid decay of field in ideal homogeneous medium is even more pronounced in cortex

Figure 4(a) – (b) COMSOL multiphysics simulation shows the current industry state-of-the-art (SOA) circular and butterfly coils and their relative electric field distributions at 1-2 mm under the coil. Figure 5(c) HFSS Maxwell 3D simulation shows advancement to the precise focality and patterning of the magnetic and induced electric fields using the proposed magnetic array.

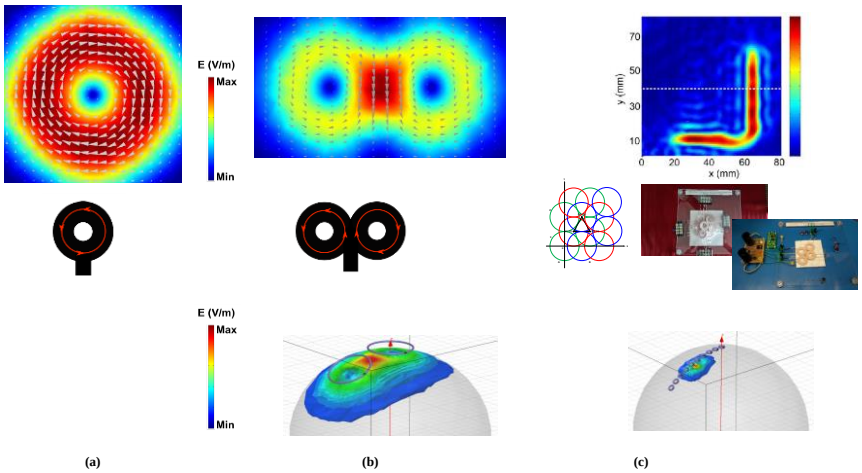

Figure 4: (a) ($\vec{E}$) induced by B-Field (flux density) on axis of a current loop at distance z and (b) SOA advancement in focality and patterning of field by proposed magnetic array [7]-[8].

3.1.1 Current TMS Issues– Unfocused Magnetic and Induced Electric Fields

When stimulation intensity is increased, unintended effects due to increased current spread can potentially be induced through the coactivation of additional nodes with confounding function, which may be completely absent at lower stimulation intensities. Overall, one needs to consider all possible effects derived from a lack of focality (both those that might artificially boost or attenuate the magnitude the predicted behavioral effects). A fundamental lack of focality is illustrated in Figure 5 in a simple lab demonstration circuit (Figure 6) that emulates exactly what the industry standard coils at lower pulsed current levels (scaled field distribution effect is the same at higher current levels).

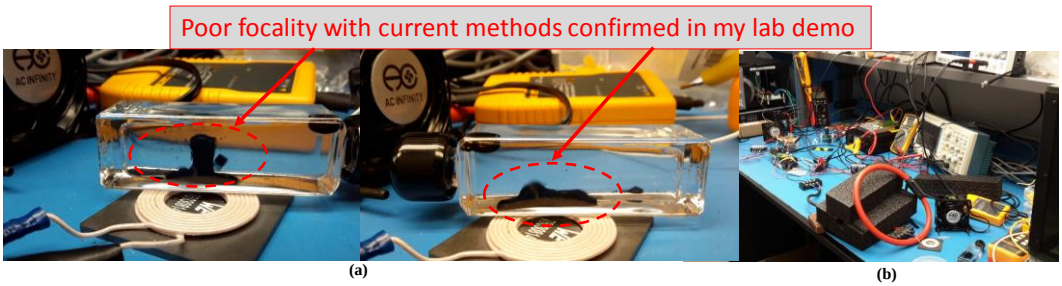

Figure 5: (a) My lab demo – still photos from movie of ferrofluids in pulsed magnetic field illustrate poorly defined field distribution (b) photo of lab bench test set-up

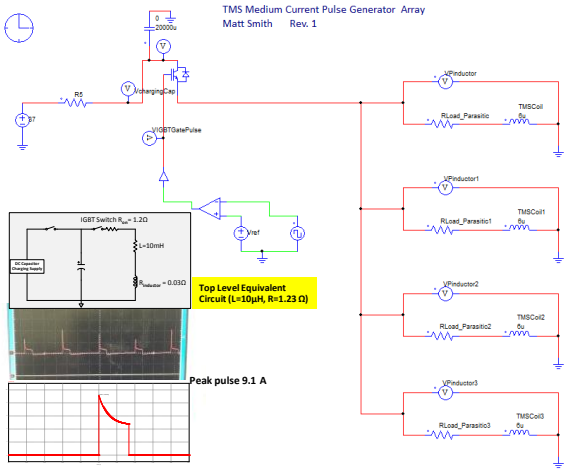

Figure 6: (a) My lab demo test schematic circuit using an IGBT switch (PSIM circuit simulation) for one test coil to demonstrate poor focality

Figure 7 (a) – (b) illustrates shows the current industry state-of-the-art (SOA) circular coil and the electric field distributions and eddy currents at 1-5mm under the coil. These patterns qualitatively agree with my lab demo observations as to the peak areas directly under the circular coil periphery. A COMSOL multiphysics simulation was used in these plots [7].

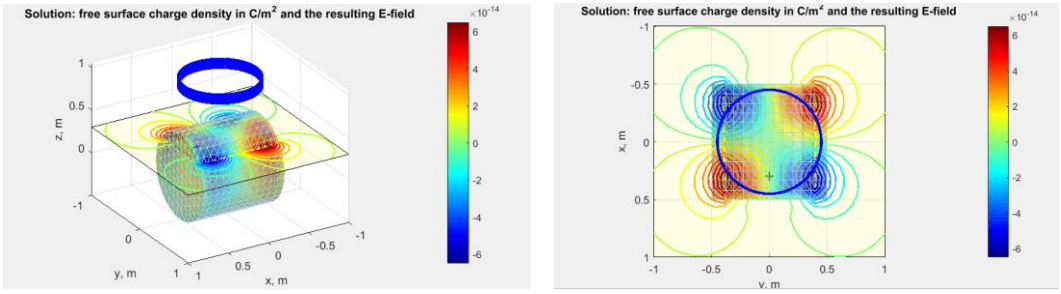

Figure 7: (a) Eddy currents (charge density C/m^3 induced by the magnetic/electric fields validate observed ferrofluid pulse shapes with strongest effect directly under the coil - illustrate poorly defined field distribution (b) z-direction looking down

Figure 8 reviews some of the considerations that must be addressed in order to properly administer a level of improved focality in TMS; (a) enhancing control and focality minimizes the likelihood of unintended effects, (b) when the beam is unfocused nodes may compete and can attenuate stimulation effects, and (c) in cascading nodes there is diminishing focality

that can alter stimulation effects. When stimulation intensity is increased, unintended effects due to increased current spread can potentially be induced through the coactivation of additional nodes with confounding function, which may be completely absent at lower stimulation intensities [12].

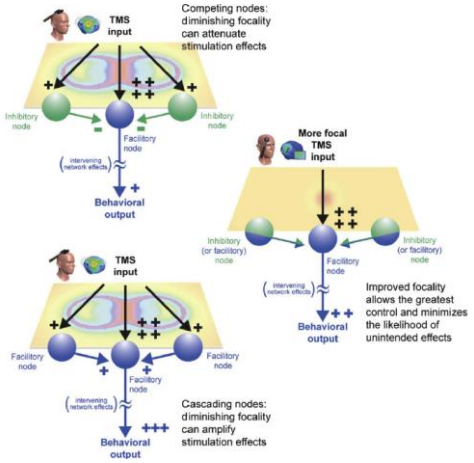

Figure 8: Improved focality allows the greatest control and minimizes the likelihood of unintended effects [12]

2.2 Induced Electric Field ($\vec{E}$)

Applying Maxwell's equations and the Lorentz gauge [11] the net induced E-field ($\vec{E}$) intensity in the tissue is comprised of two components; one primary and one secondary. The primary component, 1st term in equation (5), is the E-field directly induced by the coil and the secondary component, 2nd term in equation (5), is the E-field due to tissue-tissue interactions [13]–[15].

$$\vec{E}(\vec{r},t) = -\frac{\partial \vec{A}\,(\vec{r},t)}{\partial t} - \vec{\nabla}\,\Phi\,(\vec{r},t) \quad (6)$$

The vector potential $\vec{A}\,(\vec{r},t)$ is used to model the primary component which is directly related to the magnetic field created by the coil's rapidly changing current. The vector potential can then be determined the expression below.

$$\vec{A}\,(\vec{r},t) = \frac{\mu_o N I(t)}{4\pi} \int \frac{d\vec{l}}{|\vec{r} + \vec{r_0}|} \quad (7)$$

Where the following are defined:

- μ_o = permeability of free space
- N = # turns in the coil
- $I(t)$= time–dependent current in coil
- $d\vec{l}$ = vector oriented per direction of each current element
- $|\vec{r} + \vec{r_0}|$ = distance from each point $\vec{r}$ to the current element $\vec{r_0}$

It is assumed that the tissue permeability is approximately equal to μ_o. Equation (4) integrates each point in the volume surrounding the coil.in equation (4) so the 3D geometry of the coil and its elements are taken in to account [16].

The position of the maximum E-field ($\vec{E}$) intensity is determined by examining the membrane potential when the charge is large enough to depolarize the membrane. The E-field ($\vec{E}$) that impinges on the nerve fiber is divided in to parallel and perpendicular components as shown in Figure 9 (a). The perpendicular component is thought to have only minor impact on the membrane potential and is neglected in first order approximations [17]–[18].

Examination of the parallel part of the induced electric field on a log straight nerve sees a homogeneous field and the membrane potential is unaffected and there is no stimulation as seen in Figure 9. However, when examining a long straight nerve in a spatially varying field (Figure 9) charge is accumulated and the positions at which E-field $(\vec{\boldsymbol{E}})$ changes are the most strongly affected. These are thought to be the sites of elevated stimulation. Therefore, for straight nerves, the spatial derivative $\frac{\partial \boldsymbol{E}\,(\vec{l},t)}{\partial l}$ (parallel component) of the part of the E-field $(\vec{\boldsymbol{E}})$ that is parallel to the nerve fiber determines the site of stimulation [13]–[14].

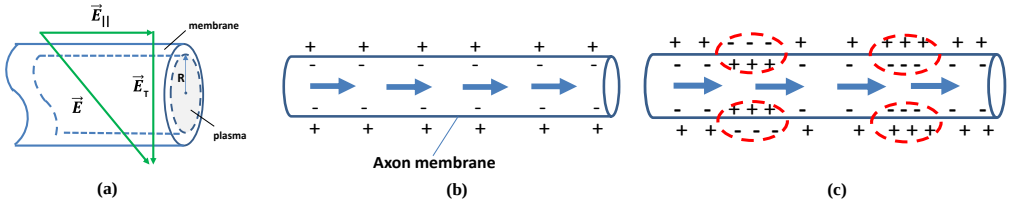

Figure 9: Nerve Fiber with E-field $(\vec{\boldsymbol{E}})$ field components and (b) Long straight nerve fiber in a homogeneous E-field $(\vec{\boldsymbol{E}})$, (c) Spatially Varying Field accumulates charge along straight nerves

This spatial derivative $\frac{\partial \boldsymbol{E}\,(\vec{l},t)}{\partial l}$ (parallel component) called the activating function of the nerve. From empirical data (*in vitro*) straight peripheral nerves are the most easily stimulated at the peaks of the spatial derivative of E-field $(\vec{\boldsymbol{E}})$.

In contrast to long straight nerves, nerve bends or discontinuities get stimulated by homogeneous fields. Also, they are stimulated and result in peaks of the spatial derivative $\frac{\partial \boldsymbol{E}\,(\vec{l},t)}{\partial l}$ (parallel component) of the part of the E-field $(\vec{\boldsymbol{E}})$ based on *in vitro* studies. Nerve bends are low-threshold points. Therefore, the stronger the E-field $(\vec{\boldsymbol{E}})$ at the bend the stronger the excitation. The same level of excitation occurs for nerve endings (terminal boutons) and branches. In a similar fashion in TMS cortical neurons are thought to be stimulated at their many bends, terminals and branches [14].

3 Neuronal Modeling of TMS Effects

The Hodgkin -Huxley equation assumes the membrane potential varies in time but not spatially as shown in eqn. (9) - (12). Therefore, this problem requires that the passive cable equation in eqn. (13) be added and combined with the Hodgkin -Huxley equation for both time and spatial components to be computed together as variables in the analysis[17]-[21].

$$C_m \frac{\partial \boldsymbol{V}}{\partial t} = -g_{Na}\, m^3 h V(V - V_{Na}) - g_K n^4 (V - V_K) - g_{Cl}(V - V_{Cl}) + \frac{I_{stim}}{2\pi a A} \qquad (9)$$

$$\frac{\boldsymbol{dm}}{\boldsymbol{dt}} = \alpha_m(V)(1 - m) - \beta_m\,(V)m \qquad (10)$$

$$\frac{\boldsymbol{dh}}{\boldsymbol{dt}} = \alpha_h(V)(1 - h) - \beta_h\,(V)h \qquad (11)$$

$$\frac{\boldsymbol{dn}}{\boldsymbol{dt}} = \alpha_n(V)(1 - n) - \beta_n\,(V)n \qquad (12)$$

where the rate constants $\alpha_m, \alpha_n, \alpha_h, \beta_m, \beta_n\, \beta_h$used in Matlab script not shown here – see appendix B

Neuronal structures can be modeled [17]-[21] using the passive cable equation expression shown in the expression

$$\tau \frac{\partial \boldsymbol{V_m}}{\partial t} + \boldsymbol{V_m} = \lambda^2 \frac{\partial^2 \boldsymbol{V_m}}{\partial a^2} + \lambda^2 \frac{\partial \boldsymbol{E_a}}{\partial a^2} \qquad (13)$$

Where the following are defined:

- $\boldsymbol{V_m}$ = change in membrane potential
- $\boldsymbol{E_a}$= projection of the E-field in that direction
- λ= passive space constant
- τ= time constant

The two equations are then combined in eqn. (20) since the problem requires that both time and space be represented in an equation that combines both. While the passive model provides the interaction between the induced E-field $(\vec{\boldsymbol{E}})$ and the nerve it does not completely describe the dynamics of the nerve stimulation. In order to fully explore the stimulation of action potentials the Hodgkin-Huxley model shown in Figure 9 is used to represent the nerve membrane to complete the chain of events that need to be modeled [17]-[21].

While the passive model provides the interaction between the induced E-field $(\vec{\boldsymbol{E}})$ and the nerve it does not completely describe the dynamics of the nerve stimulation. The active uniform cable expression is shown in eqn. (14) [22].

$$C_m \frac{\partial \boldsymbol{V}}{\partial t} = \frac{a}{2R_a} \frac{\partial^2 \boldsymbol{V_m}}{\partial x^2} - g_{Na}\, m^3 h V(V - V_{Na}) - g_K n^4 (V - V_K) - g_{Cl}(V - V_{Cl}) + \frac{I_{stim}}{2\pi a} \qquad (14)$$

$$\frac{\boldsymbol{dm}}{\boldsymbol{dt}} = \alpha_m(V)(1 - m) - \beta_m(V)m \qquad (15)$$

$$\frac{\boldsymbol{dh}}{\boldsymbol{dt}} = \alpha_h(V)(1 - h) - \beta_h(V)h \qquad (16)$$

$$\frac{\boldsymbol{dn}}{\boldsymbol{dt}} = \alpha_n(V)(1 - n) - \beta_n(V)n \qquad (17)$$

$$where\ \frac{a}{2R_a} = axial\ conductance$$

Initial Assumptions:

- Cable is terminated (i.e., sealed at the end to bound analysis)

$$\frac{\partial \boldsymbol{V}}{\partial x}(0, t) = \frac{\partial \boldsymbol{V}}{\partial x}(l, t) = 0 \qquad (18)$$

- Begins at resting state

$$V(x, 0) = V_r, \qquad m(x, 0) = m_\infty(V_r), \qquad h(x, 0) = h_\infty(V_r), \quad n(x, 0) = n_\infty(V_r) \qquad (19)$$

Figure 9 is used to represent the nerve membrane to complete the chain of events that need to be modeled [22].

$$C_m \frac{\partial \boldsymbol{V}}{\partial t} = \lambda^2 \frac{\partial^2 \boldsymbol{V_m}}{\partial x^2} - g_{Na}[\, m^3 hV + (3mm^2 h + m^3 h) v_{Na}] - g_K[\, n^4 V + (4nmn^3 h + m^3 h) v_K] - g_{Cl} V + \frac{I_{stim}(x,t)}{2\pi a} \quad (20)$$

While the passive model provides the interaction between the induced E-field $(\vec{\boldsymbol{E}})$ in the nerve fiber it does not completely describe the dynamics of the nerve stimulation in nonuniform and anisotropic media. Thus in order to fully explore the stimulation of action potentials the Hodgkin-Huxley model shown in Figure 12(a) and the passive cable model shown in Figure 12(b) are combined as shown in Figure 12(c). The objective of the model is to show, as an initial baseline for future research, that neurons are highly nonuniform in their geometries and their channels and corresponding responses to stimulation.

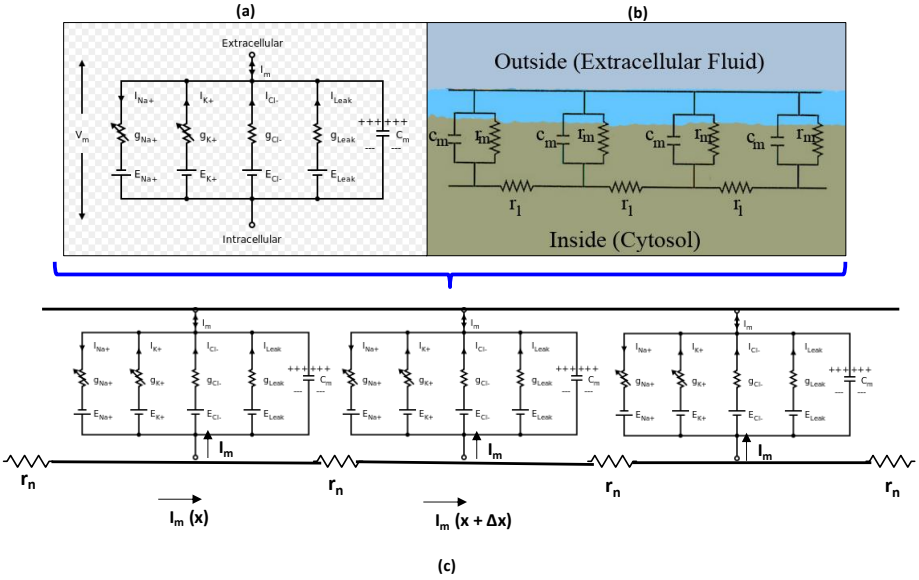

Fig. 10. (a) Hodgkin-Huxley Model [23] and (b) Passive Cable Model [23] and (c) Combined Model – Active Nonuniform Cable Model

Two spatially separate stimulation sites along a nonuniform fiber model are examined for relative excitability levels. The induced injection of an eddy current ($\boldsymbol{I_{stim}}$) constant current amplitude levels, pulse durations while changing the spatial distribution along the fiber in the direction of propagation. Figure 11 demonstrates this nonuniform effect at two different locations on the fiber for an eddy current pulse width of 1 ms, amplitude of 200pA at x=0.03 cm and x=0.06. Based on a spatial varying stimulus one point on the fiber initiates an action potential while another does not. One stimulation site is only weakly excited while the other site has enough current to initiate an action potential.

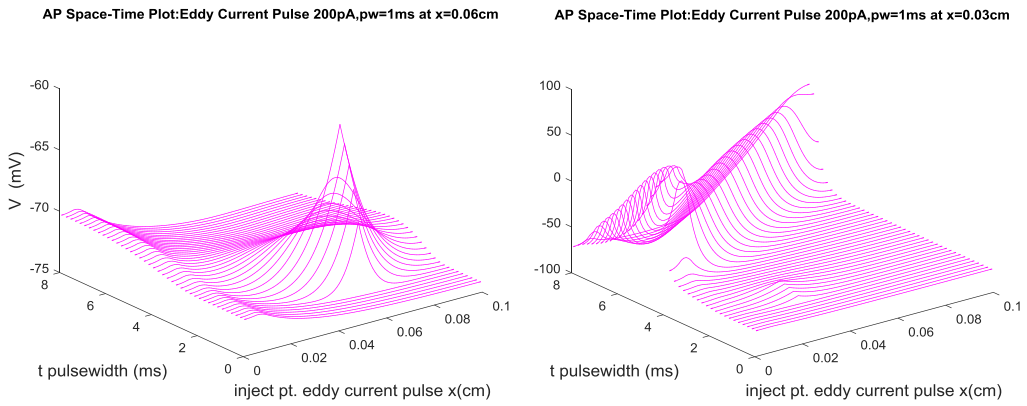

Figure 11. Active nonuniform cable shows two separate physical sites have significant differences in excitability for initiation of an action potential

When the injection eddy current is doubled to 400pA with other variables constant the two sites start to have similar levels of action potential. This makes sense since there is enough injection eddy current to excite for action potential the entire fiber length.

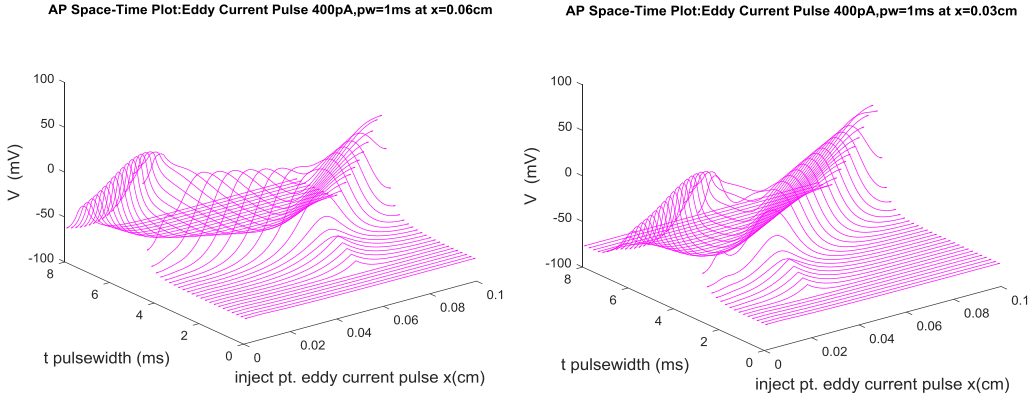

Figure 12. Active nonuniform cable shows two separate sites have significant differences in excitability for initiation of an action potential at increased injection current levels

In Figure 13 the pulse width is reduced to 0.5 ms while holding the amplitude of 200pA and evaluating the action potential at x=0.03 cm and x=0.06cm. Based on a spatial varying stimulus one point on the fiber initiates an action potential while another does not as in Figure 11. One stimulation site is only weakly excited while the other site has enough current to initiate an action potential. However, with the pulse width reduced the action potential occurs at an shorter spatial distance from the pulse.

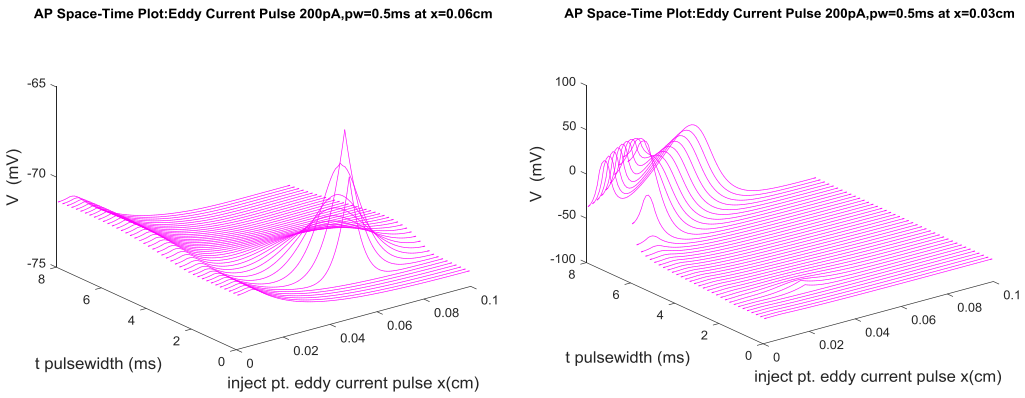

Figure 13. Active nonuniform cable shows two separate sites have significant differences in excitability for initiation of an action potential

4 Conclusion

The analysis and stimulation of a neuronal structures by electromagnetic pulses using TMS have been assessed in this study. Three key areas of bioelectromagnetic induction were identified and considered together in one model; the current pulse width, the spatial distribution of the induced electric field and the interaction with the nerve fiber. This study confirms, at a first order the level of complexity, the need for more accurate models as even a simple active nonuniform cable equation yields the need for more focality and patterning is required when writing signals to nonhomogeneous anisotropic cortical neural tissue. Thus, greater control of focality and patterning will lead to great efficacy.

Potential cortical interactions and associated effect due to TMS are reviewed in Figure 10 [12]. Pursuant to a comprehensive assessment of the current progress of theoretical treatments and models for TMS biophysical mechanisms it is evident that the hypothesis of this author still holds that one of the key weaknesses in the models is the lack of the detailed tissue complexities in the models. Biological tissue is composed of many non-homogeneous anisotropic components, such as the cellular/axonal membrane, internal organelles and the extracellular medium. Therefore, although magnetic fields can penetrate through tissue with minimal attenuation, the induced electric field is altered by these complicated tissue conductivities and this is not covered well in any of the models. Moreover, the complex geometries of neuronal structures increases the complexity the problem of effective and predictable modeling. Many of these concepts have yet to be experimentally proven and models of course at this point do not exist and at best are just beginning to emerge. Recently new computational modeling techniques has made progress in increasing the fidelity of the underlying biophysical mechanisms toward a clear path of understanding [24]-[25]. This of course, creates an exciting frontier of research that will yield benefits to mental and physical health.

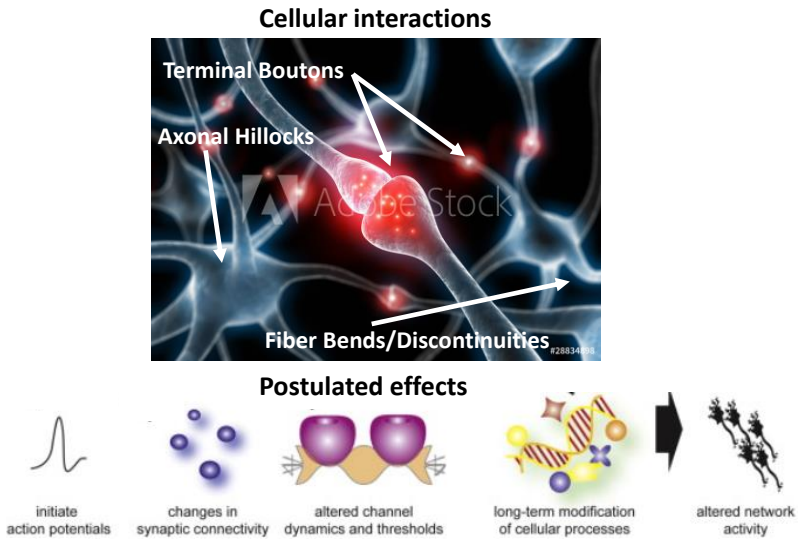

Fig. 14. Potential Cortical Interactions and postulated effects for future research and modeling [12]

Acknowledgments

I greatly appreciate my discussion with Professor Cauwenberghs on this and other related subjects. I also appreciate Jun Wang's helpful suggestion to use COMSOL Multiphysics software to simulate the bioelectromagnetics in this study.

References

[1] Barker, A.T., Jalinous, R. and Freeston, I.L. (1985) Non-invasive Magnetic Stimulation pp.1106-1107. *The Lancet*, vol. 325, issue 8437

[2] Paulus, W., Peterchev, A.V., and Ridding, M. (2013) Transcranial Electric and Magnetic Stimulation: Techniques and Paradigms pp. 329-342. In A. M. Lozano and M. Hallett, Ed. Elsevier B. V. United.Kingdom: *Handbook of Clinical Neurology- Brain Stimulation*, 3rd series, vol. 116.

[3] Feidel, D., (2015) UC San Diego Health System Transcranial Stimulation. Internet. http://www.health.ucsd.edu/specialties/psych/clinic-based/Pages/tms.aspx

[4] Piccirillo J. F. (2016) Transcranial Magnetic Stimulation for Chronic Tinnitus. pp. 506-507. *JAMA Otolaryngology–Head & Neck Surgery*: 315 (5).

[5] Hovey, C., and Jalonous, R. (2006) The Guide to Magnetic Stimulation. pp.1-8. *The Magstim Company LTD White Paper*, Part 1.

[6] MATLAB (www.mathworks.com)

[7] COMSOL Multiphysics (www.comsol.com)

[8] HFSS and Maxwell 3D (www.ansys.com)

[9] Balanis, C. (1993) Fundamentals of Engineering Electromagnetics. pp. 19-35. *Hoboken, NJ: Wiley*, 2rd edition.

[10] Cheng, D. (1993) Fundamentals of Engineering Electromagnetics. pp. 186-187. Upper Saddle River, NJ: Prentice Hall.

[11] Jackson, J. (1993) Classical Electrodynamics.pp.123-35. *Hoboken, NJ: Wiley*, 3rd edition.

[12] Wagner, T., et al (2009) Biophysical foundations underlying TMS: Setting the stage for an effective use of neurostimulation in the cognitive neuro sciences. pp. 1025-1034 CORTEX, vol. 45.

[13] Salinas, F., et al. (2007) Detailed 3D Models of the induced electric field of transcranial stimulation coils. pp. 2879-2892. *Physics in Medicine and Biology*, vol. 52.

[14] Thielscher. A., Lecture-Session 1, Topic: (no date given) Transcranial Magnetic Stimulation: From Basics to Multimodal Imaging. *Faculty of the Graduate School of Neural & Behavioral Sciences-Max Planck Institute for Biological Cybernetics*, University of Tübingen, Germany.

[15] Miranda, P. (2013) Physics of Effects of Transcranial Brain Stimulation. in A. M. Lozano and M. Hallett, Ed *Handbook of Clinical Neurology- Brain Stimulation*, 3rd series, vol. 116. pp.353-366 United Kingdom: Elsevier B. V.

[16] Yang, S., et al. (2011) Mechanisms of Magnetic Stimulation of Central Nervous System Neurons. pp. 1-18. *PLOS Computational Biology*, vol. 7, no. 3.

[17] Meffin, H., et al. (2012) Modeling extracellular electrical stimulation: I. Derivation and interpretation of neurite equations. pp.1-17 *Journal of Neural Engineering*, vol. 9.

[18] Chervyakov, A., et al. (2015) Possible mechanisms underlying the therapeutic effects of transcranial magnetic stimulation. pp.1-14 *Frontiers in Human Neuroscience*, vol. 9, no. 303.

[17] Roth, B. and Basser, P. (1990) A Model of the Stimulation of a Nerve Fiber by Electromagnetic Induction. pp. 588-597. *IEEE Transactions on Biomedical Engineering*, vol. 37, no. 6.

[18] Nagarajan, S., Durand, D. and Warman, E. (1993) Effects of Induced Electric Fields on Finite Neuronal Structures*:* pp.1175-*1188 A Simulation Study IEEE Transactions on Biomedical Engineering*, VOL. 40, NO. I I,

[19] Tang, R., et al. (2016) In Vitro Assessment Reveals Parameters-Dependent Modulation on Excitability and Functional Connectivity of Cerebellar Slice by Repetitive Transcranial Magnetic Stimulation pp. 1-12 *Scientific Report.*

[20] De Geeter, N., Crevecoeur, G., Leemans, A. and Dupré, L. (2014) Effective electric fields along realistic DTI-based neural trajectories for modelling the stimulation mechanisms of TMS pp.453-*471 IOP Publishing | Institute of Physics and Engineering in Medicine*

[21] Hodgkin, A. and Huxley, A. (1952) A quantitative description of membrane current and its application to conduction and excitation in nerve. pp. 500-544. ***J.*** *Physiol.*, vol. 117.

[22] Gabbiani & Cox (2010), Mathematics for Neuroscientists, *Academic Press - Elsevier*.

[23] www.en.wikipedia.org/wiki/Action_Potential

[24] De Geeter N., Dupré L. and Crevecoeur G. (2016) Modeling transcranial magnetic stimulation from the induced electric fields to the membrane potentials along tractography based white matter fiber tracts. *J. Neural Eng.* 13 026028 (16pp)

[25] Seo, H, et al. (2016) A Multi-Scale Computational Model of the effects of TMS on Motor Cortex (preprint not peer reviewed) *TBD*